Dual stabilization and sacrificial effect of Na2CO3 for increasing capacities of Na-ion cells based on P2-NaxMO2 electrodes

Mariyappan Sathiya, Joy Thomas, Dmitry Batuk, Vanessa Pimenta, Raghavan Gopalan, Jean-marie Tarascon

Dual stabilization and sacrificial effect of Na_2CO_3 for increasing capacities of Na-ion cells based on P2- Na_xMO_2 electrodes

Mariyappan Sathiya,[a,b,*] Joy Thomas,[b] Dmitry Batuk,[a,c] Vanessa Pimenta,[a] Raghavan Gopalan,[b] Jean- Marie Tarascon[a,d,e,*]

[a]Collège de France, 11, Place Marcelin Berthelot, 75231 Paris, France

[b]Centre for Automotive Energy Materials, International Advanced Research Centre for powder metallurgy and new materials, IITM research park, chennai-600113, India.

[c]EMAT, University of Antwerp, Groenenborgerlaan 171, B-2020, Antwerp, Belgium

[d]Réseau sur le Stockage Electrochimique de l'Energie (RS2E), FR CNRS 3459, France

[e]Sorbonne Universités - UPMC Univ Paris 06, 4 place Jussieu, F-75005 Paris, France

ABSTRACT: Sodium ion battery technology is gradually advancing and can be viewed as a viable alternative to lithium ion batteries in niche applications. One of the promising positive electrode candidates is P2 type layered sodium transition metal oxide, which offers attractive sodium ion conductivity. However, the reversible capacity of P2 phases is limited by the inability to directly synthesize stoichiometric compounds with sodium to transition metal ratio equals to 1. To alleviate this issue, we report herein the *in-situ* synthesis of P2-Na_xMO_2 ($x \leq 0.7$, M= transition metal ions) - Na_2CO_3 composites. We find that sodium carbonate acts as a sacrificial salt, providing Na^+ ion to increase the reversible capacity of the P2 phase in sodium ion full cells, and also as a useful additive that stabilizes the formation of P2 over competing P3 phases. We offer a new phase diagram for tuning the synthesis of the P2 phase under various experimental conditions and demonstrate, by *in-situ* XRD analysis, the role of Na_2CO_3 as a sodium reservoir in full sodium ion cells. These results provide insights into the practical use of P2 layered materials and can be extended to a variety of other layered phases.

Introduction:

Electrochemical energy storage devices are must as energy needs to be stored, transferred and used on demands.[1] Li-ion batteries, because of their outstanding performances, have conquered both the portable and automotive markets. Owing to the conquest of this large volume market together with the Li-ion battery ingress into renewable applications, fears about Li abundance have been voiced.[2] While over exaggerated, this had the merits to propel the search for alternate electrochemical energy storage devices.[3-5] Sodium ion batteries that work with the similar principle as lithium ion ones are considered as an interesting alternative since sodium resources are abundant in earth crust and ocean.[6] However, sodium ion batteries are limited in terms of energy and power density. Thus, achieving a comparable capacity to that of the Li-ion systems requires the identification of suitable electrode and electrolyte materials.[7, 8]

Considering the positive electrode materials, extensive research have been parted between two main categories namely Na-based poly-anionic compounds[9] and layered sodium transition metal oxides.[10, 11] Among the poly-anionic compounds, full Na-ion $Na_3V_2(PO_4)_2F_3$ /C cells with average redox potential of 3.6 V and sustained capacities of 120 mAh/g over 4000 cycles were demonstrated.[12, 13] Equally, prototypes of full Na-ion cells based on carbons and layered compounds were made as well[14] but the performances are still limited as the best layered oxide material has not been identified yet. The complexity of such Na_xMO_2 materials is rooted in their composition-structural dependence which can lead into compounds adopting a variety of structures (O3, P2, P3, O3', P3', T1 etc),[15,16] that show a wide panel of electrochemical properties. The various Na_xMO_2 structures are represented using Delmas notation with the letters P, O and T indicating the sodium coordination in prismatic, octahedral and tetrahedral site respectively, and the number signifying the total number of MO_2 layers in a unit cell.[16] Among these Na_xMO_2 phases, O3, P2 and P3 are most commonly used for sodium ion battery applications.[10,17-21] Further, the sodium ion conductivity in the P2 phase have been calculated to be

higher than in the O3 and P3 phases;[22-24] the reason why P2 phases are considered to be best suitable for high power applications.

Unfortunately, the synthesis and stabilisation of P2 over P3/ O3 phase is not straightforward owing to competing structure- stability issues.[15,16] Figure 1 shows the structure of P3, P2 and O3 phases with the zoomed part of the sodium coordination shown under each structure. The P3 phase has all sodium in one crystallographic site that shares one face with the MO_6 octahedra and the O3 structure has all sodium in its most stable position that shares edges on both sides with the MO_6 units. The stability of a specific phase is governed by the energy of the Na site, that is the sum of the inter layer repulsion between the MO_2 layers and the intra-layer repulsion between the Na ions in the Na layer. Hence, the O3 phase with reduced inter layer electrostatic repulsion is considered to be the most stable for x=1 and the P3 phase stabilizes for x~0.5 due to both sodium ion ordering and minimization of the Na-Na intra-layer repulsion.[25]

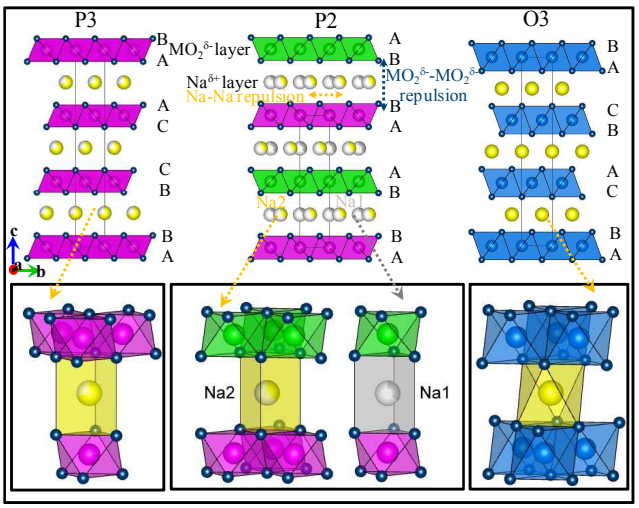

Figure 1: Structure (top) and the sodium coordination (bottom) of P3, P2 and O3 phases. The figure is plotted using the structural data from ref.[19, 26]

In contrast, P2 layered oxide has two crystallographic sites for sodium with one site (Na1) being highly destabilised by the repulsion between MO_6 and NaO_6 units that share faces together.[27] Such destabilisation reduces the stability of P2 phase over P3 and O3, hence complicates the synthesis of P2 that often requires entropy stabilisation by high temperature quenching.[28] Despite this, the quenched material is frequently contaminated by traces of Na_3MnO_4 as secondary phase.[21]

A further consideration regards the destabilisation of sodium in Na1 site which in conjunction with Na2-Na2 repulsion within the sodium layer reduces the maximum amount of sodium that can be accommodated in to the layered structure during chemical synthesis to 0.7.[27-29] This limitation stands as a capacity handicap when full Na-ion cells are assembled. Indeed, ~0.4 sodium[13] can solely be used reversibly in comparison to 0.5 or more for the O3 $NaMO_2$ phases.[14]

Interestingly, the P2 $Na_{0.7}MO_2$ phases can be electrochemically reduced to P2' Na_1MO_2 phases.[17,30-31] For this to happen in a full Na-ion cell, extra sodium must be provided to the reacting media. This can be done via the use, as previously reported, of sacrificial salts[32-34] such as carboxylate compounds, sodium azides.[35] However, the former increases the dead weight of the cell because of their high molecular weight and the latter leads to toxic products after decomposition. To circumvent these two issues at once we herein report a simple *in-situ* synthesis of P2 Na_xMO_2- Na_2CO_3 composites in which sodium carbonate acts both as a sacrificial salt and as chemical mean to stabilize the P2 phase over P3. During the course of this study, we have also surveyed the various experimental parameters that need to be considered in stabilising the P2 phase-Na_2CO_3 composite over O3 phase.

Experimental:

Synthesis: The P2 type $Na_x(Ni,Mn,Co)O_2$ layered oxides were prepared by carbonate co-precipitation[36,37] followed by solid state synthesis. The precursor (Ni, Mn, Co)CO_3 were co-precipitated using an Eppendorf Continuous flow stirred tank reactor. Stoichiometric amounts of nickel sulphate hexahydrate ($NiSO_4.6H_2O$), manganese sulphate monohydrate ($MnSO_4.H_2O$) and cobalt sulphate heptahydrate ($CoSO_4.7H_2O$) were dissolved in water to obtain a 2M aqueous solution. This solution was added drop wise with a speed of 45 ml/ h to the reactor vessel to which a base solution of 2M Na_2CO_3- 0.2M NH_4OH mixture was also added. The addition of Na_2CO_3- NH_4OH was monitored so that the pH of the reaction mixture was always maintained between 7.5 and 8 with the temperature of the bath being fixed to 55°C. The precipitated (Ni, Mn, Co) carbonate was allowed to maturate overnight at room temperature with continuous stirring and then washed with water to completely remove the sulphate anions. The precipitate was then dried at 120 °C for 12 hours in vacuum and analysed by XRD for phase purity (Figure S1 in SI). The precursor (Ni, Mn, Co)CO_3 was then mixed with sodium carbonate of required stoichiometry; 0.35, 0.4, 0.45, 0.5 and 0.55 moles of sodium carbonate was mixed with 1 mole of (Ni,Mn,Co)CO_3 to have the final Na/TM ratio (y) of 0.7, 0.8, 0.9, 1 and 1.1 respectively. The precursor mixture was calcined at 500 °C for 6 hours, followed by regrinding and second annealing at 800 °C for 12 h. The calcinations products were allowed to cool slowly to room temperature, prior to be stored in argon filled glove box. Furnace heating and cooling rate was maintained at 5 and 1 °C/min respectively.

Structural and compositional characterization: The structure of the pristine compound was analysed using a combination of the X-ray powder diffraction (XRD) and Transmission Electron Microsopy (TEM). The XRD patterns were recorded using Rigaku smartlab diffractometer and Bruker D8 diffractometer equipped with a Cu- K_α radiation source (λ = 1.54056Å). The obtained XRD patterns were refined using General Structure Analysis System Code (GSAS).[38,39] Samples for TEM were prepared by grinding the material in a mortar with anhydrous dimethyl carbonate and depositing a few drops onto holey carbon TEM grids. High resolution high angle annular dark- field scanning transmission electron microscopy (HAADF- STEM) and annular bright- field

STEM (ABF- STEM) images were recorded on a probe-aberration-corrected FEI Titan³ 80-300 electron microscope at 300 kV. Elemental distributions in the samples were studied using Energy dispersive X-ray (EDX) spectroscopy. The data were acquired in STEM mode on an FEI Osiris microscope equipped with a Super-X detector operated at 200 kV. The sample compositions were analyzed by Thermoscientific iCAP 6000 series Inductively Coupled Plasma (ICP) - emission spectrometer.

Electrochemical characterization: Electrochemical analyses of the prepared materials were done in half cell (Swagelok type), full cell (coin cell) and three electrode cell (swagelok type) assemblies. In all cases, the positive electrode was used in powder form with 85% of active material ball milled with 15% of conducting carbon. Whatman GF/D boro silicate sheets wetted with 1M sodium hexa fluoro phosphate ($NaPF_6$) in propylene carbonate (PC) solution were used as separators. The counter electrode of metallic sodium and hard carbon was used for half cell and full cell assemblies respectively. The three electrodes were assembled with hard carbon coated on an Al-sheet (loading of 5.5 mg/ cm²) as counter electrode and metallic sodium as reference electrode. Galvanostatic charge- discharge experiments were carried out using Biologic galvanostats/ potentiostats. The cells were typically cycled between 4.2 and 1.5 V at C/10 rate for half cell studies and between 4 and 0.5 V at C/50 rate for full cell and three electrode studies. The C-rate was calculated using the weight of the positive electrode (excluding conducting carbon) material. The *in-situ* XRD analysis was carried out in a specially designed cell using Be window as a current collector.

Results and discussion:

Surveying the effect of various experimental parameters (composition, temperature) on the stability of P2 phase, we first studied the effect of increasing the amount of Na (e.g adding more sodium carbonate) while maintaining the constant stoichiometry of Ni: Mn: Co (0.2: 0.6: 0.2). The resulting $Na_xNi_{0.2}Mn_{0.6}Co_{0.2}O_2$ products are termed here after as Na_xNMC262 (y=0.7 to 1.1) where 'x' represents the actual amount of sodium in the layered structure and 'y' represents the amount of sodium used in the synthesis.

Figure 2 shows the XRD patterns of the Na_xNMC262 materials prepared with y=0.7, 0.9, 1 and 1.1 hence corresponding to composites having sodium to transition metal ratio of 0.7/ 0.9/ 1 and 1.1, respectively. All XRD patterns can be refined with hexagonal P2 phase as the major phase. However, some weak peaks corresponding to traces of P3 phase are present in the y=0.7 pattern, which disappears by increasing y.

In contrast, for greater y (1 and 1.1) a second set of Bragg peaks appear that we identified as Na_2CO_3. The XRD patterns of the intermediate compositions (y=0.8, 0.9) shows single phase materials; However, a closer analysis by STEM-EDX reveals that the samples with y= 0.8 and 0.9 are not single phase but rather composites made of closely intermixed particles of Na_xNMC262 and the Na_2CO_3 phases (insets in Figure 2 and Figure S2 in SI). Such particles of Na_2CO_3 are very sparse in the y=0.7 sample. The STEM-EDX demonstrates even distribution of Na and transition metals in the Na_xNMC262 particles in all the samples (Table ST2 in SI). Overall, composites having sodium to transition metal ratio (y) of 0.7 produces P2-P3 mixture while higher ratio (y> 0.7) leads to a P2 phase coexisting with Na_2CO_3.

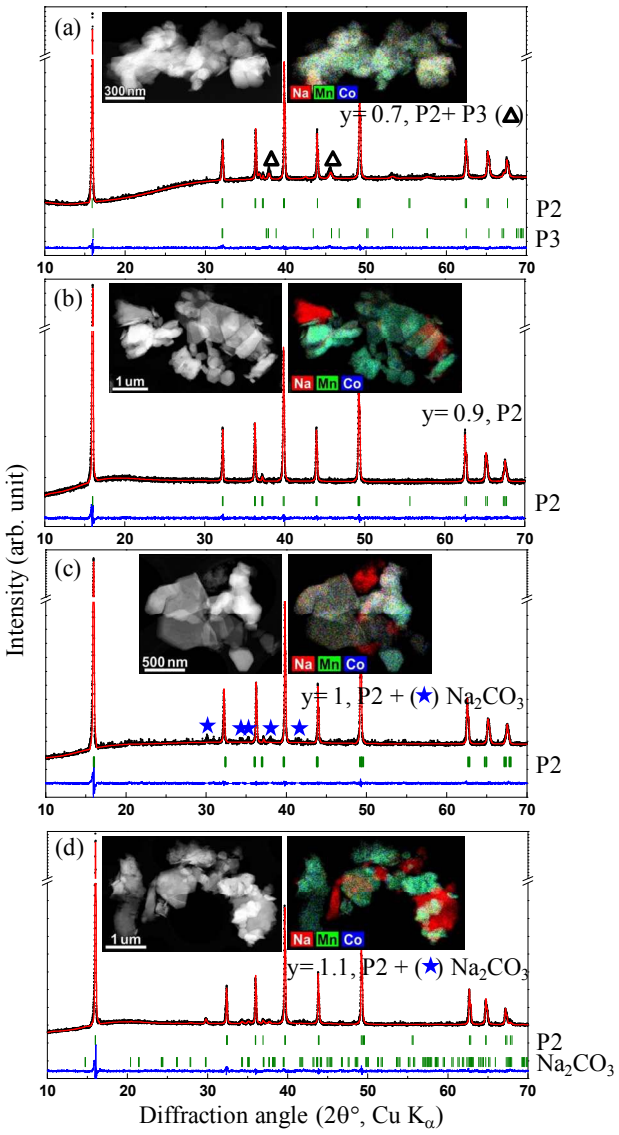

Figure 2: Powder XRD pattern of the Na_xNMC262 with Na/ TM ratio (y) of, (a) y=0.7 (b) y=0.9 c) y=1 and (d) y=1.1; black and red lines indicate the experimental and calculated XRD patterns with the blue lines showing the difference between the two. The Bragg reflections are shown by green bar lines and the refined parameters are gathered in supporting information table ST1. The insets in (a) to (d) show HAADF-STEM images and the corresponding color mix STEM-EDX elemental distribution maps (Na: red, Mn: green, Co: blue).

Further analysis of the y=0.7 sample using high resolution STEM imaging unveils that most crystals in the sample are composed of coherent intergrowths[40] of P3 and P2 type domains (Figure 3 (a)). Owing to the similarity of these structures, the intergrowths are confined to the Na layers. The thickness of the corresponding fragments varies from just two transition metal layers to a few tens of nano meters (Figure 3(a)

and Figure S3 in SI). In samples with higher sodium content (y> 0.8), the P2 structure becomes dominant (Figure 3(b)) and the P3 structure fragments are present only as occasional stacking faults in the P2 matrix. Moreover, many crystals in the y=0.7 sample demonstrate turbostratic intergrowths, where the domains are rotated with respect to each other over ~15 and 30 degrees (Figure S4 and S5 in SI). These intergrowths are absent in the samples with y> 0.8 indicating that, the Na layers responsible for such defects are Na-depleted.

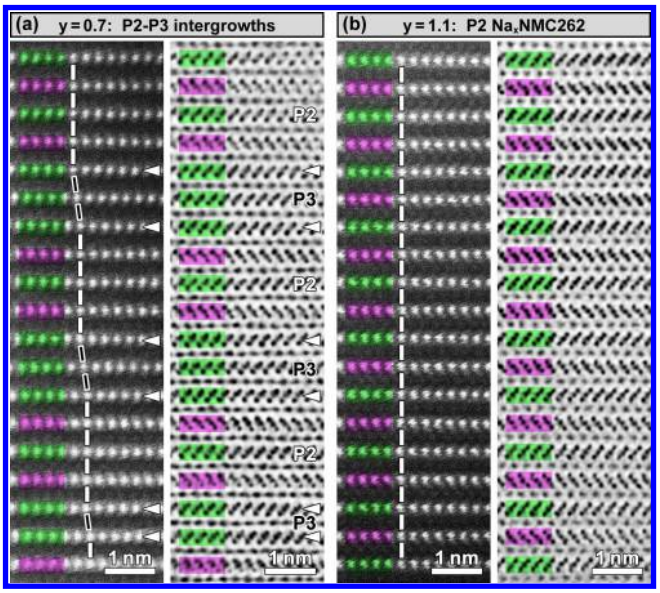

Figure 3: Typical complementary HAADF-STEM and ABF-STEM images from the y = 0.7 (a) and y = 1.1 (b) samples. The HAADF-STEM image (left panels) reveal positions of the transmission metal columns only ($I \sim Z^{1.6\text{-}1.9}$, Z is the average atomic number) while the ABF-STEM images (right panels) show both transition metal and light Na and O columns. The difference between the P2 and P3 structures in the HAADF- STEM images is only seen by the shifts of the metal columns in the adjacent layers, which are highlighted with vertical white (P2) and tilted black bars (P3). The ABF-STEM images clearly show the difference. In the P3 type structure, MO_6 octahedra in all transition metal layers are oriented in the same direction, and in the P2 structure, the orientation alternates (the layers are highlighted with the same colours as in Fig. 1).

Lastly, all materials were analysed by ICP for their Na content and the values were found to be nearly equal to the nominal composition y=0.7 to 1.1 (Table ST3 in SI), implying the Na losses during the synthesis process is minimal. The amounts of sodium carbonate in the samples were deduced gravimetrically by measuring the weight difference before and after washing the material with water. They equal 2%, 13%, 18% and 21% with y=0.7, 0.9, 1 and 1.1 respectively. Further, after washing the Na_2CO_3 in water, all materials showed a nearly same Na to metal ratio of 0.56 irrespective of the amount of sodium used in the synthesis (y). These results indicate that the amount of sodium that is stabilised in the crystal structure of P2-P3 intergrowths as well as P2 phase is nearly the same, however, the excess sodium used in the synthesis (y) helps in stabilizing the P2 over the P3 structure so that composites for y > 0.8 are solely made of the P2 and Na_2CO_3 phases.

Stabilisation of P2 over P3 phase by excess Na_2CO_3:

To understand the stabilisation/phase transition mechanism we carried-out the synthesis of P2 Na_xNMC262, y=1 sample by placing the precursor mixture pre-treated at 500°C, in a high temperature XRD Anton Paar chamber and collected XRD patterns as a function of temperature (Figure 4 (a)). Note the crystallisation of the P3 phase at around 600 °C followed by appearance of peaks related to the P2 phase when the temperature reaches 800 °C. Upon further annealing the material to 800°C for three hour, the P3 phase fully transformed into the P2 phase with nevertheless a splitting of the peaks indicative of two phases having similar structure with different lattice parameters (Figure 4b). These peaks merge together during cooling to form a P2 phase with uniform lattice. At this stage, let's recall that the (002) peak is considered as a direct indication of the *c*-axis variation. Thus, a shift of the (002) peak to high angle indicates a reduction in *c*-axis and consequently a higher amount of sodium occupying both Na1 and Na2 positions.

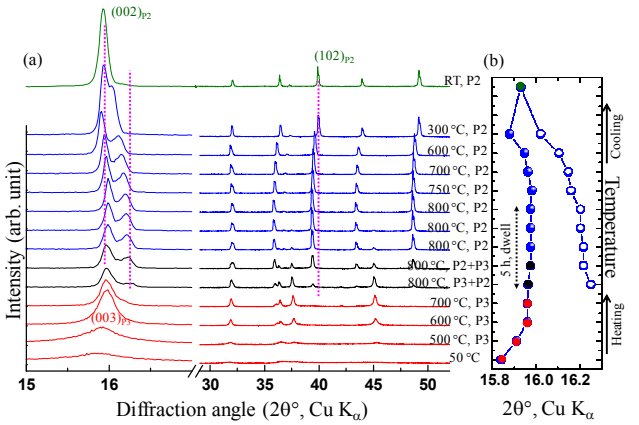

Figure 4: (a) High temperature XRD pattern of the Na_xNMC262 precursor with y= 1. The pink lines are guide to eye to follow the variations in $(002)_{P2}$ and $(102)_{P2}$ peak positions (b) Variation in $(003)_{P3}$/ $(002)_{P2}$ peak position with temperature.

This implies the presence of a Na-rich and a Na-poor P2 phase at high temperature which transforms to a more stable structure composition-wise ($Na_{0.56}$NMC262) upon cooling. Thus, regardless of the overall sodium content, the ABF- STEM images of the P2 structure fragments demonstrate preferential occupation of the Na2 positions (Figure S6 in SI). This transformation may enlist the release of Na that reacts with the CO_2 environment to form Na_2CO_3 coating with more pronounced chemical/electrochemical reactivity as we will see latter.

The feasibility of the P2 phase to host larger amounts of Na at high temperature does not come as a surprise structurally-wise since the P2 phase has two crystallographic sites for sodium (Figure 1). Thus its capability to accommodate larger amounts of sodium at

high temperature as compared to P3 phase and more so when high excess of sodium is present in the reaction mixture (as in case of y=0.8 or more). On that basis, we can understand why excess of Na favours the formation of the P2 phase which additionally preserves it to room temperature by slow cooling in contrast to previous reports.[28] At this stage, it is also worth mentioning that the P2 phases formed under such conditions are stable even after washing the excess sodium carbonate with water and re-annealing at 800 °C for 12 hours (Figure S7 in SI). Altogether, excess sodium in the reaction mixture acts as a promoter for the P3- P2 phase transformation.

Stabilisation of P2 over O3 phase:

A rather surprising result from the aforementioned synthesis work is the non-appearance of any sign of O3 phase while it was well admitted from the literature, based on structural considerations, that high sodium content favours the formation of the O3 phase over the P2 phase. To see the robustness of such finding we modified our experimental conditions by annealing the precursor (Na_2CO_3 and NMC262 carbonate pre-heated at 500 °C) to various temperatures and in different atmospheres. The results are gathered in Figure 5 (a).

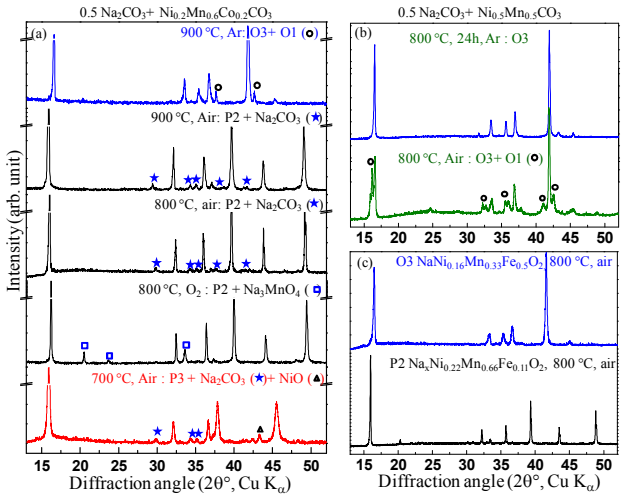

Figure 5: Powder X-ray diffraction patterns of the (a) $Na_xNMC262$, y=1.1 prepared at different temperature and in different environment, (b) $Na_xNMC550$, y=1.1 at 800 °C in air and Argon atmosphere, (c) $Na_xNi_{0.16}Mn_{0.33}Fe_{0.5}O_2$, y=1.1 and $Na_xNi_{0.22}Mn_{0.66}Fe_{0.11}O_2$, y=1.1 synthesized in air at 800 °C.

Note that at 700°C the low temperature P3 phase is formed with NiO and unreacted Na_2CO_3 impurities and it is transformed to P2 by increasing the temperature to 800 or 900 °C. This P2 $Na_xNMC262$ is always accompanied by a secondary phase that changes with the heating ambient. Na_3MnO_4 was identified as the secondary phase when heating in O_2 while Na_2CO_3 was mainly spotted when the sample was heated in air ambient. Single phase O3 samples were in contrast solely obtained for samples treated at 900 °C in inert Ar atmosphere. These results indicate the existence of a delicate balance between temperature and atmosphere for controlling P3/ P2/ O3 phase formation.

Next we embark in a survey of the effect of modifying the nature and composition of the transition metal ions on the respective formation of the P2/O3 phases. First we prepare Co-free $Na_xNi_{0.5}Mn_{0.5}O_2$ ($Na_xNMC550$) sample with (y=1) and obtained the formation of O3 ($Na_1NMC550$) phase irrespective of calcinations in air or argon (Figure 5 (b)) and of the annealing and cooling rate. Secondly, we found that attempts to replace Co by Fe with treatments of 12 hours at 800°C leads to the stabilisation of the O3 $Na_1Ni_{0.16}Mn_{0.33}Fe_{0.5}O_2$, y=1 and P2 $Na_{0.6}Ni_{0.22}Mn_{0.66}Fe_{0.11}O_2$, y=1 phases respectively (Figure 5(c)).

Altogether these results highlight a common trend with the preferentially formed structures being those enabling the transition metals to be in their most stable oxidation states. This explain why in presence of Na in excess (y=1) we obtained P2- $Na_{0.6}Ni_{0.2}^{II}Mn_{0.6}^{IV}Co_{0.2}^{III}O_2$ or O3- $Na_1Ni_{0.5}^{II}Mn_{0.5}^{IV}O_2$. Nevertheless, such a situation can be disrupt by the use of reducing ambient atmosphere (e.g. zero oxygen partial pressure gases such as argon) which tend to lower 3d metal oxidation states, hence favouring O3 rather than P2 structures for the same composition as we observed by stabilizing O3 $Na_1Ni_{0.2}^{II}Mn_{0.6}^{IV/III}Co_{0.2}^{III}O_2$ in argon and P2- $Na_{0.6}Ni_{0.2}^{II}Mn_{0.6}^{IV}Co_{0.2}^{III}O_2$ in air. Such results can be explained by recalling that the electronic repulsions between the negatively charged $MO_2^{\delta-}$ layers are minimized in O3-type structures. Thus, by lowering the average oxidation state of the 3d-metals (by modifying the ionic radii) within the $MO_2^{\delta-}$ we increase the ionic character of the M-O bond hence δ-, so favouring the O3 structure over P2 as we observed experimentally. In absence of such electronic repulsions between the $MO_2^{\delta-}$ units (when the M-O bonds are more covalent), the intra-layer Na-Na repulsion plays a main role in stabilising P2 over O3 as in P2- $Na_{0.6}Ni_{0.2}^{II}Mn_{0.6}^{IV}Co_{0.2}^{III}O_2$ (y=1).

Thus, it is tempting to take the average oxidation state of the 3d metal (n) as an indicator for guiding the formation of the O3 vs. P2 phase with n>3 or n=3 the stabilisation of the P2 and O3 phases, respectively. Thus, the use of the n parameter in our proposed phase diagram (Figure 6) , which describes in the case of a slow cool process, the relative formation of the P3 vs. P2 vs. O3 phase as a function of temperature and Na to transition metal ratio.

Within this diagram, the regions marked in yellow, blue and red represent P3, P2 and O3 phases respectively. Note that the P3 phase is formed at low temperatures irrespective of the amount of sodium and the oxidation state of the transition metal ion and is always associated with metal oxide and sodium carbonate impurities. Greater temperatures of 800- 900 °C lead to a P2 phase which is always accompanied by a P3 phase for lower sodium content. For higher Na contents the P2 phase is accompanied by Na_2CO_3 when n>3 and O3 phase when n=3. Further increasing the synthesis temperature to more than 900 °C forms pure O3 phase when n=3 and y (Na/ TM ratio) = 1; mixed P2-O3 phases with decomposed metal oxide impurities forms when n≥3 and y<1. To be complete, such a phase diagram should take into account of transition metal ratio between Ni-Mn-Co. We purposely did not include this parameter since high

ratio of large ions such as Ni^{2+} (e.g ionic consideration) for instance always give the O3 phase.

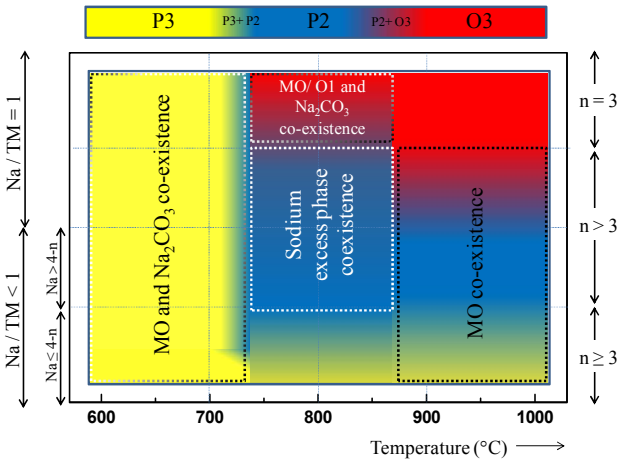

Figure 6: Synthesis phase diagram of Na_xMO_2 as a function of temperature, Na/ TM ratio and the total oxidation state on the transition metal layer (n). In the formula, M is one or more transition metal ions in which the ion such as Mn^{4+} with smaller ionic radius and high charge (+4) is in high proportion of 0.6 or more.

On the whole, the region marked in blue provides a practical tool to stabilise the P2 phase with Na_2CO_3 which is of great interest for their electrochemical performance as described next.

Electrochemical performances of the P2 $Na_xNMC262$ phases

The obtained $Na_xNMC262$ (y=0.7-1.1) materials which constitutes either the P2- P3 intergrowths (y=0.7) or the composites P2 $Na_xNMC262$- Na_2CO_3 (y=0.8-1.1) were tested for their electrochemical performances with respect to Na. The galvanostatic charge discharge profiles collected at a rate of C/10 between 1.5 and 4.2 V Vs. Na^+/Na^o are shown in Figure 7 (a-d) with all the cells having a nearly identical 2.5 V Vs. Na^+/Na^o starting potential. The y=0.7 composition shows electrochemical reactivity typical to that of P2/ P3 intergrowth phase with a charge capacity of ~70 mAh/g (4.2V) which corresponds to the removal of 0.3 Na^+ per unit formula. The subsequent discharge to 1.5 V displays a sustained reversible capacity of ~150 mAh/g over the first 20 cycles (Figure 7 (e)). The 80 mAh/g extra capacity collected during the first discharge as compared to the first charge is associated to the electrochemical insertion of sodium into P2 $Na_xNMC262$ (x<1) to form P2' $Na_xNMC262$ (x≈1).

An interesting feature on moving to y=0.9- 1.1 composites is the appearance of a plateau located at ~4V vs. Na^+/Na^o and whose amplitude increases with increasing the sample sodium content. This results in an enhancement of the charge capacities which are reaching ~90, ~140 and ~160 mAh/g for y=0.9, 1 and 1.1 respectively (Figure 7 (b) (c) and (d)), as compared to solely 70 mAh/g for the y=0.7 sample. All the cells show a reversible capacity of ~140 mAh/g on subsequent cycles as shown in capacity retention plots on the right (Figure 7 (f-h)). The corresponding derivative plots in the inset of Figure 7 (f- h) shows a sharp irreversible oxidation peak above 4V for y=0.9, 1 and 1.1 samples which does not appear on reduction, hence implying its irreversibility.

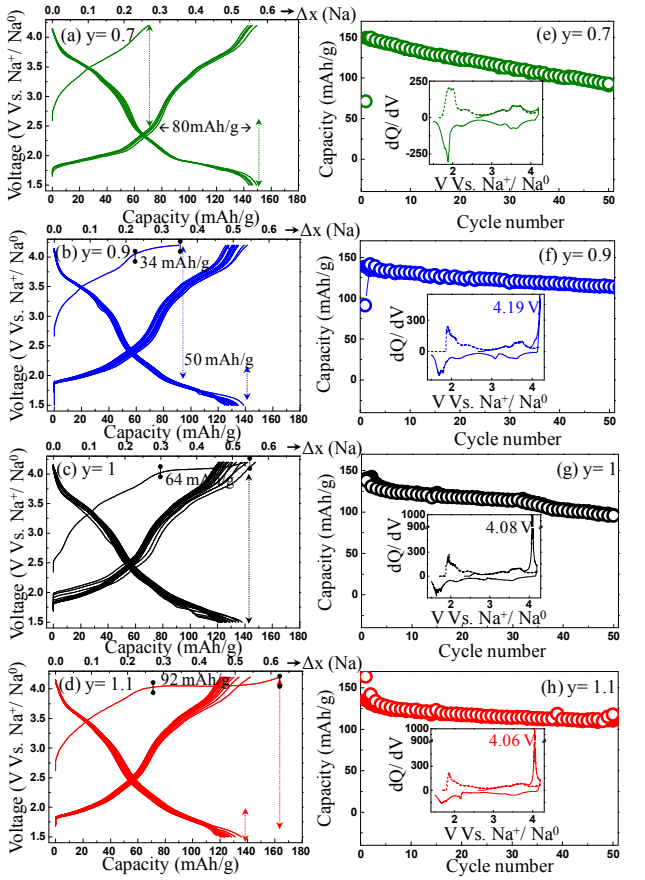

Figure 7: Galvanostatic charge- discharge profiles of P2 $Na_xNMC262$ prepared with Na/ TM ratio 'y' of (a) 0.7, (b) 0.9, (c) 1 and (d) 1.1; the difference in capacity between the first cycle charge and discharge are denoted in the cycling curves and the capacity due to the plateau at 4V are also marked in the voltage profile. (e- h) the capacity retention plots and the derivative curve as inset for (e) y=0.7, (f) y=0.9, (g) y=1 and (h) y=1.1.

Interestingly, we observed a similar irreversible oxidation peak for Na_2CO_3 powders heated at 800 °C for 12h in air (Figure 8 (a)) and placed together with 20% C in a cell that was cycled at a rate of C/50 (1 sodium removal in 50 hours). This unambiguously indicate that the irreversible charge process observed with P2 $Na_xNMC262$ (y=0.9, 1 and 1.1) above 4 V is due to the sodium carbonate secondary phase in the samples.

However, a striking difference between the bare sodium carbonate and the sodium carbonate present in the P2 $Na_xNMC262$ (y=0.9, 1 and 1.1) materials is that the former shows very limited kinetics since very slow charging process (C/50) and repeated cycling (Inset in Figure 8 (a)) were needed to barely obtain any electrochemical capacity. A maximum of 0.5 sodium can be removed from bare Na_2CO_3 on repeated cycling, however the sodium carbonate in the P2 $Na_xNMC262$-Na_2CO_3 composite provides 1.1, 1.5 and 1.8 sodium per Na_2CO_3 for y=0.9, 1 and 1.1 respectively; the values were derived by comparing the capacity from the 4 V plateau in the composite with the capacity of water washed

samples and the amount of sodium carbonate in the composite (Figure S8 in SI). Equally, the *ex-situ* addition of sodium carbonate to P2 $Na_xNMC262$ (y=0.7) by ball milling fails to show similar sodium activity (Figure 8 (b)), hence suggesting the kinetic benefits of the *in-situ* addition of Na_2CO_3 via our synthesis process. One possibility for the kinetic difference could be the proper intermixing and hence a possible interlinking of P2 phase with the Na_2CO_3 in the *in-situ* synthesized materials as shown by STEM- EDX.

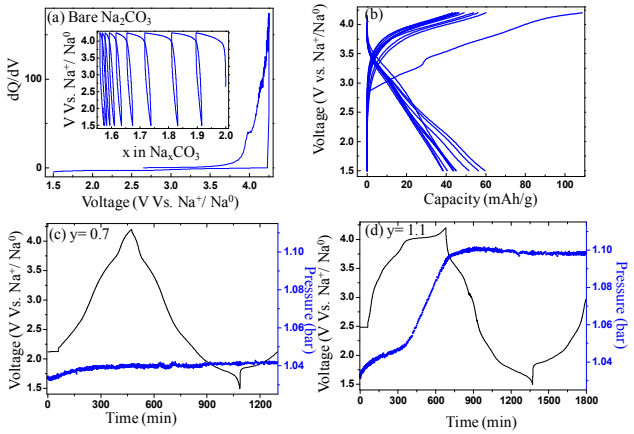

Figure 8: (a) Derivative curve of bare Na_2CO_3 cycled at C/50 rate to show the 4V decomposition peak on charge; the inset shows the voltage profile till the cell death showing maximum removal of 0.5 sodium from the sodium carbonate structure and is completely irreversible. (b) Galvanostatic charge- discharge profile of $Na_xNMC262$, y=0.7 with *ex-situ* addition of 10 % sodium carbonate and 15% conducting carbon by ball milling. (c-d) pressure cell analysis data showing the voltage and pressure variation of the cell with respect to time for (c) P2 $Na_xNMC262$, y=1.1 and (d) P2 $Na_xNMC262$, y=0.7.

Finally, to get more insights into the origin of the 4V plateau, we monitored the pressure evolution of Na half-cells using P2 $Na_xNMC262$ (y=0.7) and (y=1.1) as positive electrodes Figure 8(c and d). The cell without sodium carbonate (y=0.7) shows no increase in cell pressure throughout the cycling while the cell with y=1.1 shows initially a nearly constant pressure, which steeply increases continuously once the cell voltage reaches 4V to finally levels off at the end of charge. This is a strong indication that the gaseous product release at ~4V vs. Na^+/Na^0 is associated with the decomposition of sodium carbonate and not to electrolyte decomposition as we confirmed via ex-situ mass spectroscopy measurements which reveals mainly the presence of CO_2 as the releasing gas. The increase in cell pressure of 0.05 bar with P2 $Na_xNMC262$, y=1.1 implies a gaseous release of 1.8(5) x 10^{-5} mole. This corresponds to the amount of CO_2 released by 1.96 mg of sodium carbonate, hence suggesting that out of the 9.6 mg used in the cell assembly, 1.96 mg (nearly 20.3 %) is Na_2CO_3. Remarkably, this value nearly agrees with the 21% Na_2CO_3 weight calculated from ICP and gravimetric analysis from the same composite.

This electrochemical-driven decomposition of the sodium carbonate within the $Na_xNMC262$- Na_2CO_3 composites (y=0.9, 1 and 1.1) upon oxidation at ~4 V enlists the release of sodium ions which can be used back on reduction to form the P2' NaNMC262 from the P2 $Na_{0.7}NMC262$ phase. Under such circumstances the sodium carbonate present in our $Na_xNMC262$- Na_2CO_3 composites could act as a sodium reservoir (e.g, sacrificial salt) to provide Na^+ ions for reducing P2 $Na_xNMC262$.

To fully prove the sacrificial activity of Na_2CO_3, we have assembled full Na-ion coin cells using a hard carbon rather than metallic sodium as the negative electrode. The hard carbon coated on Al foil with a loading of 5.5 mg/ cm^2 was separated from the P2-$Na_xNMC262$ positive electrode having a loading of 13 mg/ cm^2 by glass fibre sheet soaked in 1 M $NaPF_6$ in PC as separator. Figures 9 (a) to (d) show the charge- discharge profiles of the P2 $Na_xNMC262$ (y=0.7, 0.9, 1 and 1.1) with the capacity retention plot shown as inset. Once the first charge achieved, the cells show subsequent charge and discharges that neatly superimposes upon cycling with therefore a sustainable reversible capacity which increases from 70, 93, 106 and 114mAh/g as y increases from 0.7, 0.9, 1 and 1.1, respectively. This further supports the role of Na_2CO_3 within our P2 $Na_xNMC262$-Na_2CO_3 composites as the sodium reservoir, although some doubts could subsist associated to the cell balance owing to various amounts of $Na_xNMC262$ composites.

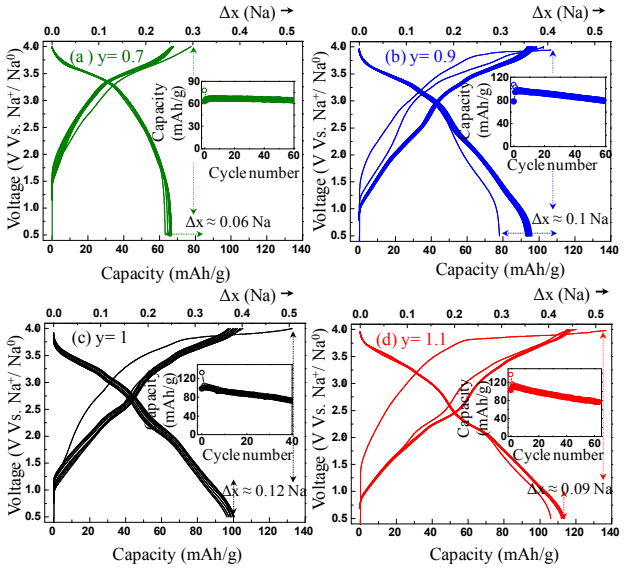

Figure 9: Voltage profile with the capacity retention plot as inset of the full cells assembled with P2 $Na_xNMC262$ phases (a) y=0.7, (b) y=0.9, (c) y=1 and (d) y=1.1; the reversible capacity of the full cells increased with increasing y and hence increasing amount of Na_2CO_3 sacrificial salt in the composite.

To remove this doubt and directly follow the Na insertion/de-insertion in positive and negative electrodes separately, we assembled 3-electrodes Na-ion cells using Swagelok hardware and a Na reference electrode while maintaining similar positive, negative electrodes and electrolytes as before. The charge/discharge profiles for cells using P2 $Na_xNMC262$ (y=0.7, 0.9, 1 and 1.1 respectively) as positive electrodes are reported in Figures 10 (a) to (c) and in Figure S9.

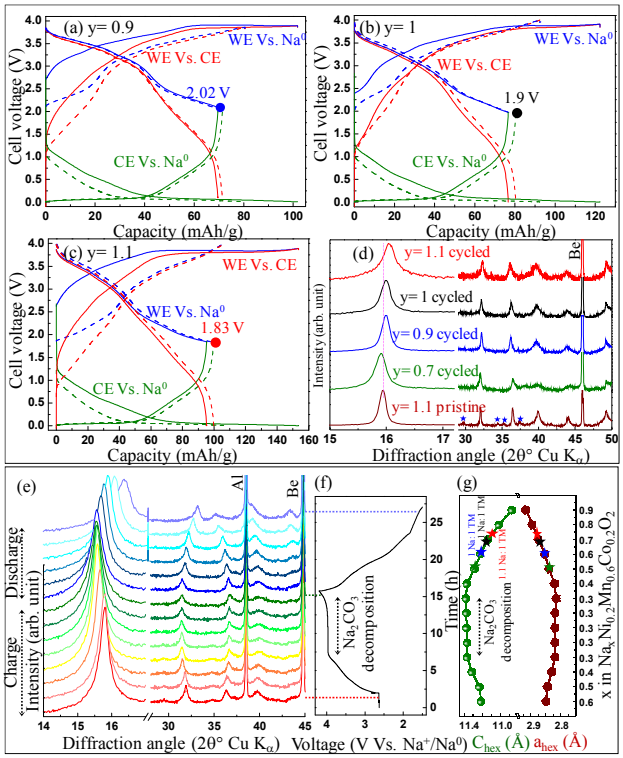

Figure 10: Voltage profiles of the P2 $Na_xNMC262$ with (a) y=0.9, (b) y=1 and (c) 1.1 samples in three electrode assembly; the notations WE and CE represents working P2 $Na_xNMC262$ and counter hard carbon electrodes respectively. (d) *Ex-situ* XRD pattern of the discharged samples at the end of two cycles in three electrode assembly in comparison with the pristine $Na_xNMC262$, y=1.1. The XRD pattern from 2θ= 30- 60 ° are zoomed twice to that of 15- 17 ° for clarity reasons. (e) *in-situ* XRD profile of the P2 $Na_xNMC262$, y=1.1 material in sodium half cells and the (f) the corresponding charge-discharge profile of the *in-situ* cell. (g) Lattice parameter variation of the P2 $Na_xNMC262$ on charge- discharge derived from the *in-situ* XRD analysis and profile fitting using GSAS. The green, blue, black and red stars marked in (g) are lattice parameters derived from (d) of the full cells corresponding to P2 $Na_xNMC262$ with y=0.7, 0.9, 1 and 1.1 respectively.

Note first that the voltage profile of the negative hard carbon electrode vs. Na^+/Na^o (green curve) is alike the one measured on Na-half (C/Na) cells irrespective of the positive electrode used.[41] The overall reversible capacity with increasing 'y' is also clearly visible as before. The plots provide additional information regarding the end discharge voltage of the positive electrode (blue curve). This end of discharge voltage changes from 3, 2.02, 1.92 and 1.8 V for y=0.7, 0.9, 1 and 1.1 respectively. The corresponding derivative plot indicating an increasing capacity of the redox process of the 1.8 V peaks that is associated with the reduction of the P2 and P2' phase with increasing y (Figure S10 in SI).

The discharged product at the end of second cycle was analysed by XRD. From the XRD patterns (Figure 10 (d), we observed a continuous shift of the (00*l*) peaks to higher angles and the (10*l*) peaks to lower angles with increasing y. From profile matching we could deduce based on the hexagonal space group *P63/mmc* that such a shift was simultaneously corresponding to a contraction and expansion of the *c* and *a* lattice parameters, respectively, with increasing y. To follow such lattice parameter variation, we have carried out *in-situ* XRD analysis of the $Na_xNMC262$ (y=1.1) samples in sodium half cells. The XRD pattern with the corresponding charge- discharge profile and the lattice parameter variation in the hexagonal space group are given in Figure 10 (e), (f) and (g) respectively. As expected,[17] there is a reduction of the *a* and an increase of the *c* lattice parameters upon increasing the cell voltage to 4.1 V, but the collected X-ray diffraction pattern remain identical through the 4.1 V plateau implying once again that this plateau is mainly due to the sodium carbonate decomposition. The lattice parameter variation of the P2 phase follows a reverse trend with decreasing *c* lattice and increasing *a* lattice on discharge.

Additionally, by using the lattice parameters variation of the *in-situ* $Na/Na_xNMC262$ (y=1.1) as reference (Figure 10 (g)) and reporting the lattice parameters of the discharged products $Na_xNMC262$ (y=0.7/ 0.9/ 1/ 1.1) recovered by dismantling full cells at voltages denoted by green, blue, black and red dots in Figure 10 (d), we could calculate the final composition of the discharged product to be $Na_{0.5}NMC262$, $Na_{0.6}NMC262$, $Na_{0.67}NMC262$ and $Na_{0.74}NMC262$ for y=0.7, 0.9, 1 and 1.1 respectively. This nearly 40% increase in the sodium content between the fully discharged y=0.7 and y=1.1 samples clearly demonstrate that Na_2CO_3 is acting as a sacrificial salt by providing more Na^+ ions to the system. However, it is worth mentioning that we could never observe a complete conversion of P2 to P2' with the compositions (y ≤ 1.1) studied herein, most likely due to the partial utilisation of sodium ion for the SEI formation in the negative hard carbon electrode.

In summary, through a survey of various synthesis conditions (temperature, composition, nature of M,..) we have successfully synthesized the layered P2-Na_xMO_2 (x≤ 0.6, M= transition metal ions)- Na_2CO_3 phase against the competing P3 and O3 phases. Moreover, we reported that the resulting Na_xMO_2-Na_2CO_3 composites show an improved capacity in Na-ion full cells as compared to cells using Na_2CO_3 free electrodes. Such an improvement is ascribed to the presence of Na_2CO_3, which acts as a sacrificial salt, as demonstrated, via complementary XRD, pressure and 3-electrode measurements. We believe that such a finding can be extended to any other sodium layered oxides Na_xNMC, thus providing a flexible tuning strategy for enhancing the performances of Na-ion full cells based on P2 positive electrodes. However, caution should be taken as the sodium carbonate decomposition is associated with release of gaseous products and need to be removed after the formation cycle. Secondly, the continuous phase transition from P2 to P2' phase with possible contribution from Mn^{4+}/Mn^{3+} redox on long cycling may lead to poor capacity retention. One possible solution to anticipate these foreseen limitations could consist in identifying suitable 3d metal to improve the capacity retention. We must therefore recognize, owing to the 3d-metal cationic diversity together with their wide relative ratio combination, there is complexity in finding the delicate balance between annealing temperature, annealing atmosphere, cooling process ,proper amount of Na_2CO_3 to stabilize the P2 phase and their dependence on

electrochemical activity. Such a task is time consuming hence calling for the development of combinatorial chemistry/robotics to speedily screen these various systems.

ASSOCIATED CONTENT

Supporting information. 10 figures, and three tables showing XRD and electrochemical studies of P2 $Na_xNMC262$- Na_2CO_3 composite. This material is available free of charge via the Internet at http://pubs.acs.org.

AUTHOR INFORMATION

Corresponding Authors

* jean-marie.tarascon@college-de-france.fr (J.M-T); sathiya.mariyappan@college-de-france.fr (M.S)

Author Contributions

All authors have given approval to the final version of the manuscript.

ACKNOWLEDGMENT

M.S, J. T and R. G acknowledge the financial support received from Department of Science and Technology (DST-SERC), Government of India under the funding from TRC Grant Agreement No. AI/1/65/ARCI/2014. The authors are thankful to Dr. Sundararajan, Chairman, TRC and Dr. G. Padmanabham, Director, ARCI for helpful discussions. Initial microscopy analysis by Dr. M. B. Sahana, Dr. Prabu and Mr. Ravi Gautham of ARCI are greatly acknowledged. The elemental analysis by Dr. Domitille Giaume, IRCP – ENSCP,Chimie Paris tech, Paris is greatly acknowledged.

REFERENCES

1. Armand, M.; Tarascon, J. M. Building better batteries. Nature. 2008, 451, 652-657.
2. Tarascon, J.-M. Is lithium the new gold? Nat Chem. 2010, 2, 510-510.
3. Larcher, D.; Tarascon, J. M. Towards greener and more sustainable batteries for electrical energy storage. Nat Chem. 2015, 7, 19-29.
4. Grey, C. P.; Tarascon, J. M. Sustainability and in situ monitoring in battery development. Nat Mater. 2017, 16, 45-56.
5. Perry, M. L.; Weber, A. Z. Advanced Redox-Flow Batteries: A Perspective. J. Electrochem. Soc. 2016, 163, A5064-A5067.
6. Kundu, D.; Talaie, E.; Duffort, V.; Nazar, L. F. The Emerging Chemistry of Sodium Ion Batteries for Electrochemical Energy Storage. Angew Chem Int edit. 2015, 54, 3431-3448.
7. Yabuuchi, N.; Kubota, K.; Dahbi, M.; Komaba, S. Research Development on Sodium-Ion Batteries. Chem. Rev. 2014, 114, 11636-11682.
8. Kubota, K.; Komaba, S. Review—Practical Issues and Future Perspective for Na-Ion Batteries. J. Electrochem. Soc. 2015, 162, A2538-A2550.
9. Ni, Q.; Bai, Y.; Wu, F.; Wu, C. Polyanion-Type Electrode Materials for Sodium-Ion Batteries. Adv. Sci. 2017, 4, 1600275-n/a.
10. Han, M. H.; Gonzalo, E.; Singh, G.; Rojo, T. A comprehensive review of sodium layered oxides: powerful cathodes for Na-ion batteries. Energy Environ Science. 2015, 8, 81-102.
11. Naoaki, Y.; Shinichi, K. Recent research progress on iron- and manganese-based positive electrode materials for rechargeable sodium batteries. Science and Technology of Advanced Materials. 2014, 15, 043501.
12. Fang, Y.; Zhang, J.; Xiao, L.; Ai, X.; Cao, Y.; Yang, H. Phosphate Framework Electrode Materials for Sodium Ion Batteries. Adv. Sci. 2017, 4, 1600392.
13. Dugas, R.; Zhang, B.; Rozier, P.; Tarascon, J. M. Optimization of Na-Ion Battery Systems Based on Polyanionic or Layered Positive Electrodes and Carbon Anodes. J. Electrochem. Soc. 2016, 163, A867-A874.
14. Oh, S.-M.; Oh, P.; Kim, S.-O.; Manthiram, A. A High-Performance Sodium-Ion Full Cell with a Layered Oxide Cathode and a Phosphorous-Based Composite Anode. J. Electrochem. Soc. 2017, 164, A321-A326.
15. Delmas, C.; Fouassier, C.; Hagenmuller, P. Stabilite relative des environnements octaedrique et prismatique triangulaire dans les oxydes lamellaires alcalins AxMO2 ($x \leqslant 1$). Mater Res Bull. 1976, 11, 1483-1488.
16. Delmas, C.; Fouassier, C.; Hagenmuller, P. Structural classification and properties of the layered oxides. Physica B+C. 1980, 99, 81-85.
17. Berthelot, R.; Carlier, D.; Delmas, C. Electrochemical investigation of the P2–NaxCoO2 phase diagram. Nat Mater. 2011, 10, 74-80.
18. Carlier, D.; Cheng, J. H.; Berthelot, R.; Guignard, M.; Yoncheva, M.; Stoyanova, R.; Hwang, B. J.; Delmas, C. The P2-$Na_{2/3}Co_{2/3}Mn_{1/3}O_2$ phase: structure, physical properties and electrochemical behavior as positive electrode in sodium battery. Dalton Transactions. 2011, 40, 9306-9312.
19. Sathiya, M.; Hemalatha, K.; Ramesha, K.; Tarascon, J. M.; Prakash, A. S. Synthesis, Structure, and Electrochemical Properties of the Layered Sodium Insertion Cathode Material: $NaNi_{1/3}Mn_{1/3}Co_{1/3}O_2$. Chem. Mater. 2012, 24, 1846-1853.
20. Kalapsazova, M.; Ortiz, G. F.; Tirado, J. L.; Dolotko, O.; Zhecheva, E.; Nihtianova, D.; Mihaylov, L.; Stoyanova, R. P3-Type Layered Sodium-Deficient Nickel–Manganese Oxides: A Flexible Structural Matrix for Reversible Sodium and Lithium Intercalation. ChemPlusChem. 2015, 80, 1642-1656.
21. Yabuuchi, N.; Kajiyama, M.; Iwatate, J.; Nishikawa, H.; Hitomi, S.; Okuyama, R.; Usui, R.; Yamada, Y.; Komaba, S. P2-type $Na_x[Fe_{1/2}Mn_{1/2}]O_2$ made from earth-abundant elements for rechargeable Na batteries. Nat Mater. 2012, 11, 512-517.
22. Mo, Y.; Ong, S. P.; Ceder, G. Insights into Diffusion Mechanisms in P2 Layered Oxide Materials by First-Principles Calculations. Chem. Mater. 2014, 26, 5208-5214.
23. Yabuuchi, N.; Komaba, S. Recent research progress on iron- and manganese-based positive electrode materials for rechargeable sodium batteries. Science and Technology of Advanced Materials 2014, 15, 043501.
24. Guo, S.; Sun, Y.; Yi, J.; Zhu, K.; Liu, P.; Zhu, Y.; Zhu, G.-z.; Chen, M.; Ishida, M.; Zhou, H. Understanding sodium-ion diffusion in layered P2 and P3 oxides via experiments and first-principles calculations: a bridge between crystal structure and electrochemical performance. NPG Asia Mater. 2016, 8, e266.
25. Radin, M. D.; Van der Ven, A. Stability of prismatic and octahedral coordination in layered oxides and sulphides intercalated with alkali and alkaline-earth metals. Chem. Mater. 2016, 28, 7898-7904.
26. Chagas, L. G.; Buchholz, D.; Vaalma, C.; Wu, L.; Passerini, S. P-type $Na_xNi_{0.22}Co_{0.11}Mn_{0.66}O_2$ materials: linking synthesis with structure and electrochemical performance. J. Mater. Chem. A. 2014, 2, 20263-20270.
27. Delmas, C.; Braconnier, J.-J.; Fouassier, C.; Hagenmuller, P. Electrochemical intercalation of sodium Na_xCoO_2 bronzes. Solid State Ionics. 1981, 3/4, 165-169.
28. Lei, Y.; Li, X.; Liu, L.; Ceder, G. Synthesis and Stoichiometry of Different Layered Sodium Cobalt Oxides. Chem. Mater. 2014, 26, 5288-5296.
29. Hinuma, Y.; Meng, Y. S.; Ceder, G. Temperature-concentration phase diagram of P2- Na_xCoO_2 from first principle calculations. 2008, 77, 224111.
30. Han, M. H.; Gonzalo, E.; Sharma, N.; Lopez del Amo, J. M.; Armand, M.; Avdeev, M.; Garitaonandia, J. J. S.; Rojo, T. High performance P2-phase $Na_{2/3}Mn_{0.8}Fe_{0.1}Ti_{0.1}O_2$ cathode material

for ambient-temperature sodium-ion batteries. Chem. Mater. 2016, 28, 106-116.
31. Talaie, E.; Duffort, V.; Smith, H. L.; Fultz, B.; Nazar, L. Structure of the high voltage phase of layered P2- $Na_{2/3-z}[Mn_{1/2}Fe_{1/2}]O_2$ and the positive effect of Ni substitution on its stability. Energy Environ. Sci. 2015, 8, 2512.
32. Guyomard, D.; Tarascon, J. M. The carbon/$Li_{1+x}Mn_2O_4$ system. Solid State Ionics. 1994, 69, 222-237.
33. Shanmukaraj, D.; Grugeon, S.; Laruelle, S.; Douglade, G.; Tarascon, J.-M.; Armand, M. Sacrificial salts: Compensating the initial charge irreversibility in lithium batteries. Electrochem. commun. 2010, 12, 1344-1347.
34. Zhang, B.; Dugas, R.; Rousse, G.; Rozier, P.; Abakumov, A. M.; Tarascon, J.-M. Insertion compounds and composites made by ball milling for advanced sodium-ion batteries. Nat Commun. 2016, 7, 10308.
35. Singh, G.; Acebedo, B.; Cabanas, M. C.; Shanmukaraj, D.; Armand, M.; Rojo, T. An approach to overcome first cycle irreversible capacity in P2-$Na_{2/3}[Fe_{1/2}Mn_{1/2}]O_2$. Electrochem. Commun. 2013, 37, 61-63.
36. Lee, D. K.; Park, S. H.; Amine, K.; Bang, H. J.; Parakash, J.; Sun, Y. K. High capacity $Li[Li_{0.2}Ni_{0.2}Mn_{0.6}]O_2$ cathode materials via a carbonate co-precipitation method. J. Power sources. 2006, 162, 1346-1350.
37. Park, S. H.; Kang, S. H.; Belharouak, I.; Sun, Y. K.; Amine, K. Physical and electrochemical properties of spherical $Li_{1+x}(Ni_{1/3}Co_{1/3}Mn_{1/3})_{1-x}O_2$ cathode materials. J. Power sources. 2008, 177, 177-183.
38. Larson, A. C.; Dreele, R. B. V., General Structure Analysis System (GSAS). Los Alamos National Laboratory Report LAUR 2000, 662.
39. Toby, B. H., EXPGUI, a graphical user interface for GSAS. Journal of Applied Crystallography 2001, 34, 210-213.
40. Dolle, M.; Patoux, S.; Doeff, M. M. Layered manganese oxide intergrowth electrodes for rechargeable lithium batteries.1. Substitution with Co or Ni. Chem. Mater. 2005, 17, 1036-1043.
41. Komaba, S.; Murata, W.; Ishikawa, T.; Yabuuchi, N.; Ozeki, T.; Nakayama, T.; Ogata, A.; Gotoh, K.; Fujiwara, K. Electrochemical Na Insertion and Solid Electrolyte Interphase for Hard-Carbon Electrodes and Application to Na-Ion Batteries. Advanced Functional Materials. 2011, 21, 3859-3867.

Insert Table of Contents artwork here